Desalination and Water Treatment
www.deswater.com

doi: 10.5004/dwt.2023.29417

289 (2023) 163–179
March

Poly(methacrylic acid) surface modified magnetite nanoparticles for dispersive solid-phase adsorption of chlorpyrifos pesticide from aqueous solutions

Mandana Nozari, Shahab Shariati*

Department of Chemistry, Rasht Branch, Islamic Azad University, Rasht, Iran, Fax: +981333402718; emails: shariaty@iaurasht.ac.ir (S. Shariati), mandana.nozari93@gmail.com (M. Nozari)

Received 9 September 2022; Accepted 26 February 2023

ABSTRACT

Population growth and the increasing need for agricultural and food products, enhance usage of pesticides, which are special water pollutants. In this study, we synthesized poly(methacrylic acid) modified magnetite nanoparticles (Fe_3O_4@PMA MNPs) to remove chlorpyrifos organophosphate pesticide from aqueous samples. The structure of synthesized MNPs was characterized by vibrating sample magnetometer, field-emission scanning electron microscopy, Fourier-transform infrared spectroscopy, X-ray diffraction, and dynamic light scattering. Effective operational parameters such as pH, adsorbent mass, contact time and ionic strength were evaluated at four levels by Taguchi fractional factorial design method (OA_{16}). Under the optimum conditions (pH = 5, adsorbent content = 2 g·L^{-1}, ionic strength = 0.005 mol·L^{-1} and 30 min contact time), the removal efficiency of 89.8% was obtained. The kinetic studies at two concentrations of 5 and 25 mg·L^{-1} showed that chlorpyrifos removal followed the pseudo-second-order kinetic model (R^2 = 0.99, q_{eq} = 11.31 mg·g^{-1}) confirming diffusion plays a key role in determining the rate of adsorption process. The adsorption equilibrium data were investigated by linear and non-linear forms of four isotherm models, and the results showed good accordance with the Dubinin–Radushkevich isotherm model (R^2 = 0.99). From the thermodynamic studies, $\Delta H°$, $\Delta S°$, $\Delta G°$, and E_a of adsorption process were obtained as 9.665 kJ·mol^{-1}, 40.25 J·mol^{-1}·K^{-1}, –2.326 kJ·mol^{-1} and 8.677 kJ·mol^{-1}, respectively. The results revealed that the adsorption process was endothermic ($\Delta H° > 0$) and spontaneous ($\Delta G° < 0$). The obtained values of $\Delta H°$, $\Delta G°$ and E_a confirmed the physisorption nature of interaction. The calculated E_a and sticking probability (S^*) showed the endothermic adsorption process and high probability of sticking to the surface, respectively. This study showed that Fe_3O_4@PMA MNPs are suitable adsorbents for removing chlorpyrifos pesticide from aqueous solutions.

Keywords: Magnetite; Nanoparticles; Methacrylic acid; Chlorpyrifos; Adsorption; Removal

1. Introduction

Chemical pesticides have helped to increase the agricultural products by controlling pests and diseases and investigating insect-borne diseases in the human health sector. Their inappropriate use and entry of their residues in the food chain have an essential impact on the ecosystem via polluting of soil, air, land, and surface waters. They cause concern because of their epidemic in the living and working environment [1].

Chlorpyrifos is an organophosphate insecticide that has mild mercaptan odor and is used on crops, animals, and buildings, and in other settings, to kill a number of pests, including insects and worms [2].

Chlorpyrifos has been widely used in agriculture, horticulture, grape farming, forestry, and in a wide range

* Corresponding author.

of crops, in residential and non-residential uses, to control beetles, fleas, and cattle ticks and pests in stables. Compared to alternative products, this pesticide is widely used because of its overall effectiveness, and therefore it is often chosen as an alternative to organochlorine pesticides [3]. Chlorpyrifos has many destructive effects on the skin, nervous, respiratory, digestive systems, and fetus growth and development and is considered moderately hazardous to humans (Class II) by the World Health Organization. Chougule et al. [4] showed that chlorpyrifos played a pivotal role in the pathophysiology of pulmonary dysfunctions and increased apoptosis in the lungs of mice. Another study by Tian et al. [5] showed that chlorpyrifos causes skeletal malformations in the fetus. Also, Verma et al. [6] stated that exposure to chlorpyrifos causes oxidative stress in rat tissue. The use of chlorpyrifos was banned in USA from 2016, in the European Union from 2020 and in a number of other countries [7].

Different methods are used to remove various pollutants from water environments. The most important methods are reverse osmosis, ion replacement, electrodialysis, electrolysis, advanced oxidation, and adsorption. Adsorption is a fast, cheap, and widely used method [8]. In this method, a suitable adsorbent is used to remove pollutants. The best advantages of adsorption processes are simplicity and flexibility of design, ability to remove various pollutants, and easy and facile production and operation [9]. Nowadays, magnetite nanoparticles (MNPs) have demonstrated a high ability to adsorb pollutants due to their minimal size, the high surface-to-volume ratio, their separation by an external magnetic field and the flexibility in the synthesis of diverse adsorbents containing proper functional groups [10]. Up to now, numerous magnetic nanostructures were successfully used for preconcentration or removal of various organic [11–13] and metallic ions and inorganic spices [14–18]. The co-precipitation method that was firstly developed by Khalafallah, is known as the oldest methods for synthesis of MNPs. The advantages of this method are its low expenses, not being time-consuming, and allowing the researcher to make large amounts of nanoparticles in low reaction volumes [19]. Different protection and coating methods prevent unintentional oxidation, aggregation of nanoparticles and ultimately maintain their unique properties. For this purpose, various coatings including carbon, silica, metal, metal oxide, organic polymers, and surfactants are used [20,21]. During surface modification, MNPs can be functionalized with a particular group such as –OH, –COOH, and $–NH_2$ [22,23].

Several studies have been conducted to remove pesticides by using various adsorbents including permethrin removal from water by a composite of chitosan-ZnO nanoparticles as adsorbent [24] cypermethrin removal from contaminated water using nanomaterial [25], paraquat removal by core-shells of magnetite nanoparticles decorated by SBA-3-SO_3H mesoporous silica [26], chlorpyrifos removal using chitosan-graphene oxide composite from water solutions [27], diazinon removal from water using multi-walled carbon nanotubes [28], cypermethrin removal from water using collagen-based CuO nanoparticles [29], and removal of diazinon using bentonite acid treated with dilute H_2SO_4 solutions [30].

In this study, Fe_3O_4, MNPs were synthesized and after surface modification by poly(methacrylic acid) (PMA), they were used to remove the chlorpyrifos pesticide from water solutions for the first time. The idea of using surface-modified MNPs as adsorbent is due to their high adsorption capacity, low cost, and simple separation with applying external magnetic fields. For this purpose, the magnetite nanoparticles (Fe_3O_4, MNPs) were synthesized by the co-precipitation method and modified by methacrylic acid. Then, the effect of different variables on the adsorption process was investigated by Taguchi orthogonal array design method. Also, isotherm, kinetic, and thermodynamic models were evaluated to show the rate, capacity of adsorption, and the effect of temperature on the process.

2. Experimental set-up

2.1. Chemicals

The chemicals including iron(III) chloride hexahydrate ($FeCl_3·6H_2O$), iron(II) chloride tetrahydrate ($FeCl_2·4H_2O$), ammonia (NH_3), ethanol (EtOH, C_2H_5OH), methanol (MeOH, CH_3OH), doubly distilled water, sodium hydroxide (NaOH), hydrochloric acid (HCl, 37 wt.%), methacrylic acid ($C_4H_6O_2$), sodium dodecyl sulfate (SDS, $C_{12}H_{25}NaO_4S$), potassium persulfate ($K_2S_2O_8$) and sodium chloride (NaCl) were bought with high purity from Merck (Darmstadt, Germany), and Fluka (Buchs, Switzerland). Chlorpyrifos pesticide (Fig. 1, $C_9H_{11}Cl_3NO_3PS$, phosphorothioate-pyridinyl-2-trichloro-6,5,3-0 diethyl-0,0, M_W = 350.6 g·mol^{-1}, density, 1.398 g·cm^{-3} (at 43.5°C); melting point, 43°C; boiling point, 160°C; log*p* (octanol/water), 4.96; pK_a = 4.55; colorless crystals) with 98% purity was prepared from Sigma-Aldrich (Milwaukee, WI, USA).

At first, chlorpyrifos stock solution (1,000 mg·L^{-1}) was prepared in EtOH. Other solutions used for adsorption studies were prepared by dilution of this stock solution in distilled water. During the experiment, 0.1 and 0.01 molar (M) solutions of HCl and NaOH were used to regulate the pH of the solutions, and all experiments were carried out at ambient temperature.

2.2. Instruments and equipment

All adsorption measurements were obtained using an Agilent Cary 60 UV-Vis spectrophotometer (USA). For adsorption measurements of chlorpyrifos, 302 nm was selected as the maximum absorption wavelength (λ_{max}). The pH of the solutions was adjusted using a pH meter (inoLab pH 7110, WTW, Germany) equipped with a combined glass electrode. A magnetic stirrer (Labinco model L81, Netherlands) was used to stir the pesticide solutions. A 1.4 T permanent

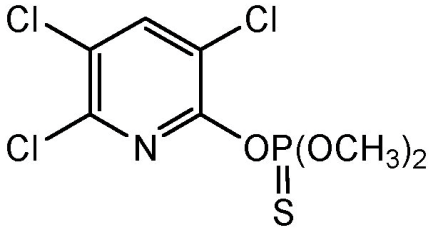

Fig. 1. Chemical structure of chlorpyrifos.

super magnet (5 cm^3 × 3 cm^3 × 1 cm^3) was used for magnetic separations. Digital scale (FA2004B model) with 0.0001 g accuracy was utilized for weighing materials. The electric oven (Memmert model INE 400, Germany) was applied to dry the nano adsorbents. Nitrogen gas with 99% purity was used to remove dissolved oxygen. The Fourier-transform infrared spectra (FT-IR) of the samples were obtained using a Fourier-transform infrared (FT-IR) instrument (Shimadzu 8900 FT-IR spectrometer, Japan) with KBr pellets in the wavenumber range of 400–4,000 cm^{-1} to characterize the functional groups on the surface of MNPs. To study the structure of crystalline materials, X-ray diffraction pattern with X-ray diffraction (XRD) device (*X'*Pert PRO MPD PANalytical Company, Netherlands) with Cu-Kα radiation source at 40 kV voltage and 30 mA current was used to record XRD patterns in the air at ambient temperature in a wide-angle range (2θ = 10°–80°). For investigating the surface morphology of the synthesized MNPs, the field-emission scanning electron microscopy (FE-SEM) was used (LEO1430VP model, co-product of Germany and England). A vibrating sample magnetometer (VSM, Kashan Daneshpajouh Magnetism Company) was used to measure the magnetic properties of synthesized MNPs. Dynamic light scattering (DLS, 180°NANO-flex model, Particle Metrix, Germany) was used to determine the size and shape of MNPs in the solution.

Non-linear kinetic and isotherm models were solved in Originpro v8.6 and kinetic and isotherm parameters were obtained.

2.3. Preparation of poly(methacrylic) acid coated magnetite nanoparticles (Fe_3O_4@PMA MNPs)

2.3.1. Synthesis of Fe_3O_4 MNPs

Magnetite nanoparticles (Fe_3O_4 MNPs) were synthesized by the co-precipitation method via addition of a mixture of Fe^{3+} and Fe^{2+} ions (with a molar ratio of 2:1) to ammonia solution. Briefly, 50 mL solution of iron salts (4 g $FeCl_2{\cdot}4H_2O$, 10.4 g $FeCl_3{\cdot}6H_2O$) containing 1.5 mL HCl 37%) was prepared. This solution was transferred into a separatory funnel and deoxygenated by purging N_2 gas to prevent oxidation (15 min) and heated to 80°C. This solution was added drop by drop into a three-necked flask containing 250 mL ammonia solution (4.5 M) during 60 min under N_2 gas purging and 80°C solution temperature with vigorous stirring (1,000 rpm). After formation of the black precipitate of $Fe_3O_4^-$ MNPs, the mixture was stirred in the same condition for 10 min. At the end of this period, the black precipitate of MNPs was separated by the 1.4 Tesla magnet, washed four times with deionized water, and maintained in 0.1 M NaOH solution for 1 h to prevent agglomeration or accumulation of MNPs. In the last step, the black sediments were collected using the magnet, washed three times with distilled water, and dried in an oven at 90°C for 24 h [31].

2.3.2. Coating of Fe_3O_4 MNPs with poly(methacrylic) acid (Fe_3O_4@PMA MNPs)

Poly(methacrylic) acid synthesis was performed on the magnetite core, based on Zeng et al. method [32]. For this purpose, 1 g MNPs was added to 200 mL distilled water and stirred for 30 min. Then, 2 g sodium dodecyl sulfate (SDS) was added to the solution and the solution was stirred for 30 min. After adding 1 mL methacrylic acid (MA), at the pH = 3, 2 g $K_2S_2O_8$ was added to the mixture and the solution was stirred under N_2 gas for 2 h. The resulting MNPs were separated by magnets and dried in the air. Finally, the applicability of the obtained MNPs was investigated in removing chlorpyrifos pesticide from aqueous samples. For this purpose, Taguchi orthogonal array method was used. By using potassium peroxydisulfate initiator at the mentioned temperature and in the presence of gas, the anion radical readily polymerizes the double bond. Therefore, the created polymer from the double bonding part is joined to Fe_3O_4, and the carbon group does not disappear.

2.4. Dispersive solid phase adsorption of chlorpyrifos pesticide using Fe_3O_4@PMA MNPs

The synthesized Fe_3O_4@PMA MNPs were applied for the removal of chlorpyrifos pesticide from the aqueous solutions. To obtain the best absorption wavelength of chlorpyrifos in the spectrophotometric measurements, the UV-Vis absorption spectra of chlorpyrifos solution (200 $mg{\cdot}L^{-1}$) was obtained in the wavelength range of 200–800 nm. Based on the UV-Vis spectra, 302 nm was chosen as the best wavelength for chlorpyrifos measurements.

All of the batch adsorption experiments of chlorpyrifos were performed at room temperature (r.t.) with 50 mL solutions containing a certain concentration of chlorpyrifos (0.1–100 $mg{\cdot}L^{-1}$). Firstly, the pH and ionic strength of the solutions were adjusted by dropwise addition of 0.1 M HCl or NaOH solutions, and addition of NaCl, respectively (pH = 5, ionic strength = 0.005 $mol{\cdot}L^{-1}$). Then, a proper amount of the adsorbent (0.1 g) was added to the chlorpyrifos solution, and the solution was stirred vigorously on a magnetic stirrer for a period of time (30 min). Upon completion of the removal experiments, a permanent super magnet was applied to separate the Fe_3O_4@PMA MNPs. The chlorpyrifos removal efficiency (*R*%) was obtained by UV-Vis spectrophotometric measurements of residual solution at 302 nm using a proper calibration curve (calibration equation in the concentration range of 1–30 $mg{\cdot}L^{-1}$ was obtained as $A = 0.0221C–0.0243$ with regression coefficient $R^2 = 0.9987$). The removal efficiency of chlorpyrifos was calculated as follows:

$$\%\text{Removal} = \frac{C_0 - C_t}{C_0} \times 100 \quad (1)$$

where C_0 and C_t are initial and residual concentrations of chlorpyrifos after treatment with adsorbent, respectively. Fig. 2 shows the schematic of using Fe_3O_4@PMA MNPs for chlorpyrifos removal.

3. Results and discussion

3.1. Structural characterization of Fe_3O_4@PMA nano adsorbent

VSM, FE-SEM, XRD, FT-IR, and DLS instruments were used to characterize the synthesized Fe_3O_4@PMA MNPs. The FT-IR spectra of nano adsorbent is shown in Fig. 3a. The

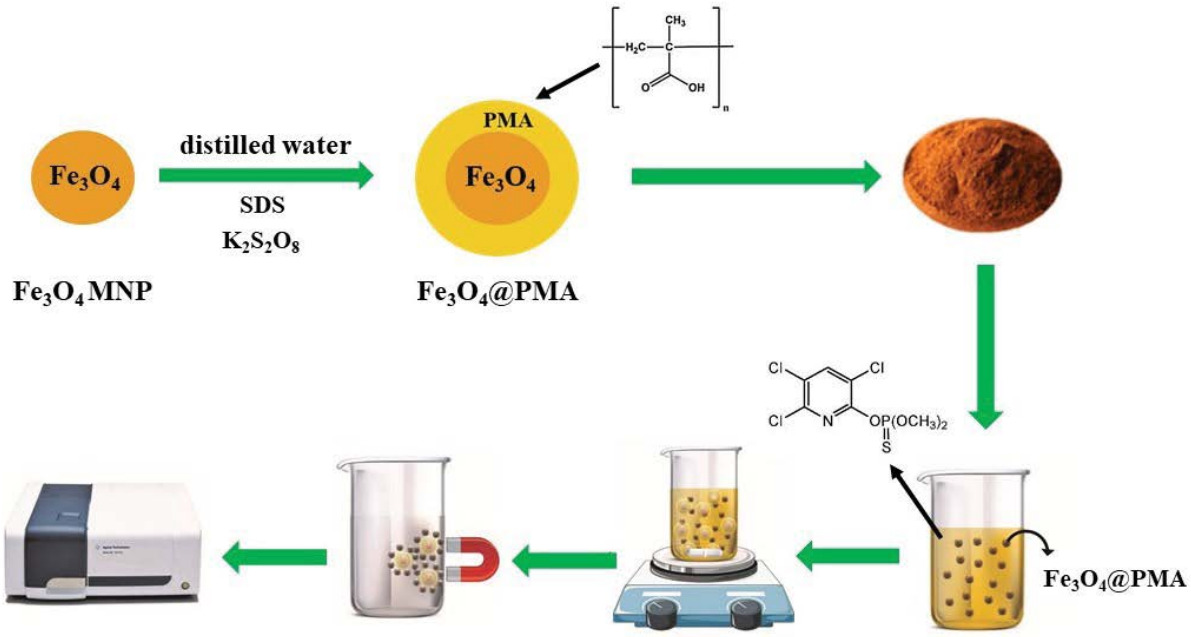

Fig. 2. Schematic for the preparation of Fe_3O_4@PMA MNPs and its application in chlorpyrifos removal.

absorption bands at 973 and 1,056 cm^{-1} are related to the C–O stretching vibrations. Bands at 2,848 and 2,918 cm^{-1} are assigned to the stretching vibrations of C–H bond. The highly broad absorption that occurs in the region of 2,400–3,500 cm^{-1} is the most significant property of a carboxylic acid's spectrum. The existence of polyhydroxyl (OH^-) groups in the structure is demonstrated by the presence of a high intensity wide absorption band in the range of 3,000–3,650 cm^{-1} (specially 3,471 cm^{-1}). The peak of roughly 1,209 cm^{-1} corresponds to the presence of $(CH_2)_n$ [32]. The absorption bands at 572 and 628 cm^{-1} that are related to the Fe–O stretching vibrations indicate the presence of magnetite in the structure of Fe_3O_4@PMA MNPs [26].

Fig. 3b shows the XRD pattern of Fe_3O_4@PMA MNPs. The reflection peaks at the at 2θ = 30°, 35°, 43°, 53°, 57°, 63° and 75° are related to the reflections with Miller indexes of (2 2 0), (3 1 1), (4 0 0), (4 2 2), (5 1 1), (4 4 0) and (5 3 3), respectively, indicating the existence of Fe_3O_4 nanoparticles with the cubic crystal structure in the structure of synthetic nano adsorbent, which is compatible with the diffraction pattern of pure Fe_3O_4 (JCPDS No. 19–629) [23,26].

Fig. 3c and d show the FE-SEM and the histogram images of the synthesized Fe_3O_4@PMA MNPs to obtain the shape, morphology and size distribution of particles. The FE-SEM images with different magnifications showed the production of almost spherical particles with diameters smaller than 40 nm. The histogram of particle-size distribution confirmed the majority of the particle-size distribution lies in the region of 30–50 nm.

The VSM analysis was carried out while the applied magnetic field was swept from the –10 to 10 kOe to investigate the magnetic property of the synthesized Fe_3O_4@PMA MNPs (Fig. 3e). According to the findings, the amount of saturation magnetization is 38 $emu \cdot g^{-1}$, which is less that the bare Fe_3O_4 MNPs (50 to 78 $emu \cdot g^{-1}$) [26]. However, this amount is enough to properly separate MNPs by applying a magnetic field. The decreased saturation magnetization of Fe_3O_4@PMA MNPs is related to the PMA layer covered the surface of magnetite core.

The hydrodynamic diameter of the synthesized Fe_3O_4@PMA MNPs in suspension was investigated by DLS (Fig. 3f). The graph depicts the intensity obtained by the device's sensors from laser light scattering on the sample in various dimensions. According to the findings, the dispersed synthesized MNPs showed average hydrodynamic diameters about 567 nm with a polydispersity index of PI = 3.51. The difference in the obtained size in DLS and FE-SEM is related to this fact that the DLS data shows the hydrodynamic diameter of the particles in the solution and the possibility of aggregation of particles.

3.2. Optimizing the factors affecting the dispersive solid phase adsorption efficiency of chlorpyrifos pesticide

In order to obtain the best removal efficiency with minimum experiments, Taguchi fractional factorial design was utilized to evaluate the experimental variables affecting the chlorpyrifos removal efficiency. Four affecting experimental parameters including solution pH 4, 5, 6 and 7, adsorbent amount 0.03, 0.05, 0.08 and 0.1 g, contact time 5, 10, 15 and 30 min and ionic strength as NaCl concentration 0, 0.005, 0.01, and 0.05 M were studied at four levels by Taguchi orthogonal array method. All optimization experiments were done using 50 mL solution containing 25 $mg \cdot L^{-1}$ chlorpyrifos. According to the number of main factors, the OA_{16} (4^4) was designed by Design-Expert software, and 16 experiments were designed for optimizing the adsorption parameters (Table 1). To avoid any personal or subjective bias, the order of the experiments was randomized. The removal efficiency for each trial was calculated

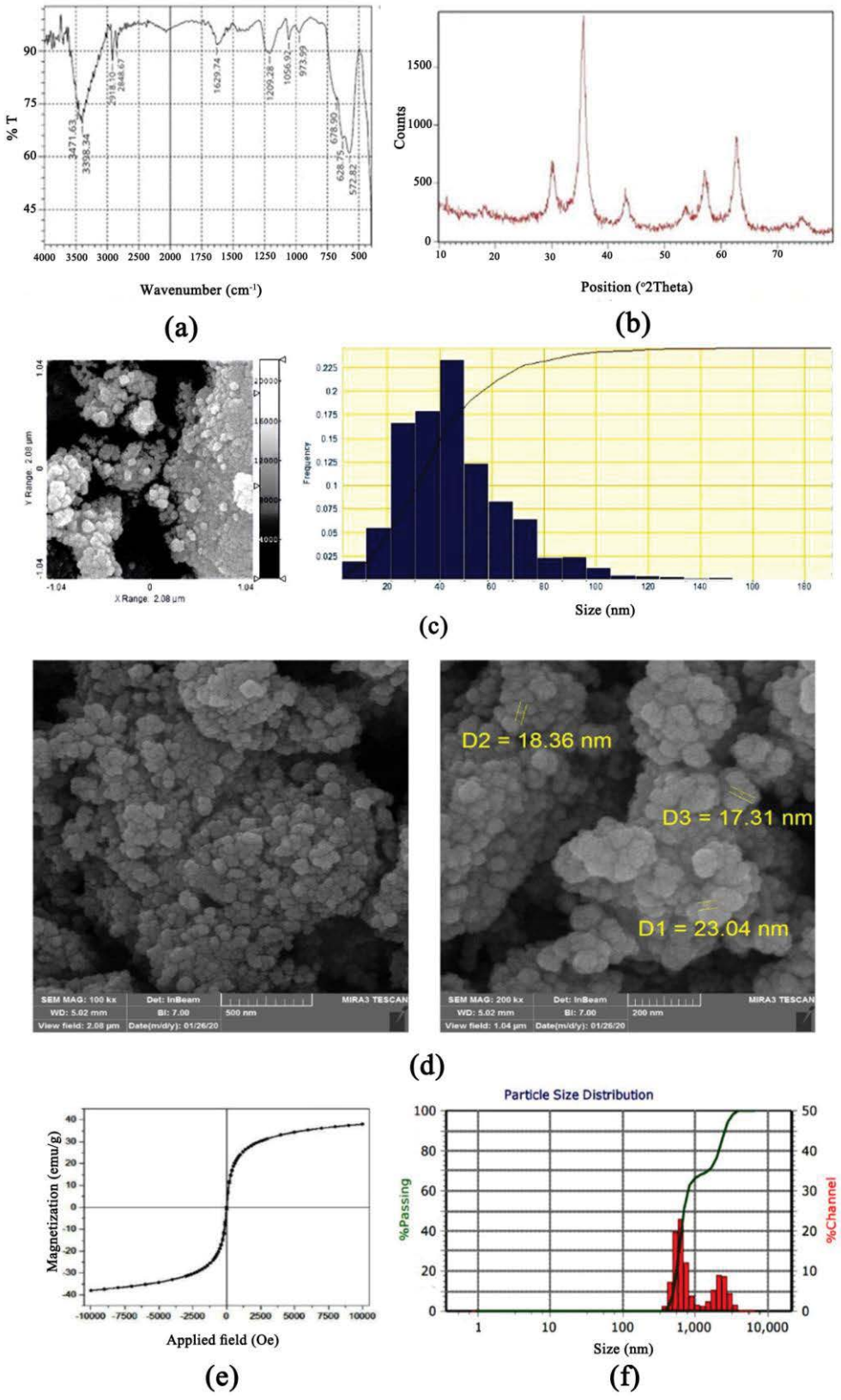

Fig. 3. (a) Fourier-transform infrared spectra, (b) X-ray diffraction spectra, (c) histogram diagram of particle-size distribution, (d) field-emission scanning electron microscopy image, (e) vibrating sample magnetometer curve, and (f) dynamic light scattering pattern of the synthesized Fe_3O_4@PMA MNPs.

via measuring the UV-Vis absorbance of the residual solution using a calibration curve. The designed experiments and the mean of removal efficiencies of each parameter in various levels (r_1, r_2, r_3, and r_4) were calculated and summarized in Table 1. To explore the repeatability of the removal process under the optimal conditions (pH = 5, adsorbent weight = 0.1 g, ionic strength = 0.005 mol·L^{-1}, and contact time = 30 min), this pattern was repeated three times and the mean removal efficiency was acquired about 95%.

Table 1
Taguchi matrix for adsorptive removal of chlorpyrifos

Run	Contact time (min)	Sorbent mass (g)	pH	Ionic strength (mol·L^{-1})	Removal (%)
1	5	0.03	4	0	18.50
2	10	0.05	4	0.005	82.93
3	15	0.08	4	0.01	83.66
4	30	0.1	4	0.05	90.35
5	15	0.03	5	0.005	71.16
6	30	0.05	5	0	89.44
7	5	0.08	5	0.05	74.42
8	10	0.1	5	0.01	89.81
9	30	0.03	6	0.01	84.74
10	15	0.05	6	0.05	87.09
11	10	0.08	6	0	70.98
12	5	0.1	6	0.005	87.28
13	10	0.03	7	0.05	43.11
14	5	0.05	7	0.01	42.02
15	30	0.08	7	0.005	80.58
16	15	0.1	7	0	83.84
r_1	55.55	54.38	68.86	65.69	–
r_2	71.71	75.37	83.46	80.49	–
r_3	81.44	77.41	82.52	75.06	–
r_4	86.28	87.82	62.39	73.74	–

The pH of the solution is an essential variable that influences the electrostatic interaction between the adsorbent/adsorbate system [26]. To investigate the effect of solution pH on the chlorpyrifos removal efficiency, different pHs 4, 5, 6, 7 in the Taguchi experimental design were evaluated. According to the optimization results (Fig. 4) at pH 5, this adsorbent showed the maximum removal efficiency of 83.5%. There are no significant differences in removal efficiency in pH levels slightly higher than this. By reducing the pH of the solution, the concentration of H^+ ions in the solution increases which causes more positive charge on the chlorpyrifos (pK_a = 4.55). Therefore, electrostatic repulsions occur between the protonated Fe_3O_4@PMA MNPs adsorbent and the positive charges of chlorpyrifos, resulting in little pesticide adsorption. As a result, the pH of the adsorption medium should be raised to avoid this.

The adsorption of positively charged pesticide on the adsorbent should be increased by reducing the concentration of H^+ ions as well as increasing the negative charge density on its surface. The intensity of chlorpyrifos adsorption depends on the pH of the solution. The carbon atom of chlorpyrifos works as an electrophilic center at pH ≥ 7, and with increasing the concentration of OH^- ions at higher pHs, the pesticide is decomposed. On the one hand, detoxification occurs via the H_3O^+ nucleophilic attack at pH ≤ 2, but on the other hand, in milder acidic situations, detoxification occurs at a slower rate. Actually, at low pHs, H_3O^+ breaks the bond between the aromatic rings and generates a nontoxic molecule. The van der Waals force adsorbs chlorpyrifos, and hydrogen bonds are formed between the pesticide and adsorbent functional groups, acting as a driving agent for chlorpyrifos adsorption from water. As a result, in this investigation, the optimum pH was 5 [33,34].

The adsorbent amount is an essential parameter that has a significant effect on the adsorption process. Different amounts of adsorbent ranging from 0.03 (0.6 g·L^{-1}) to 0.1 g (2.0 g·L^{-1}) were studied to investigate the effect of adsorbent amount (Fig. 4). As seen, the removal efficiency of chlorpyrifos improves when the amount of adsorbent is increased.

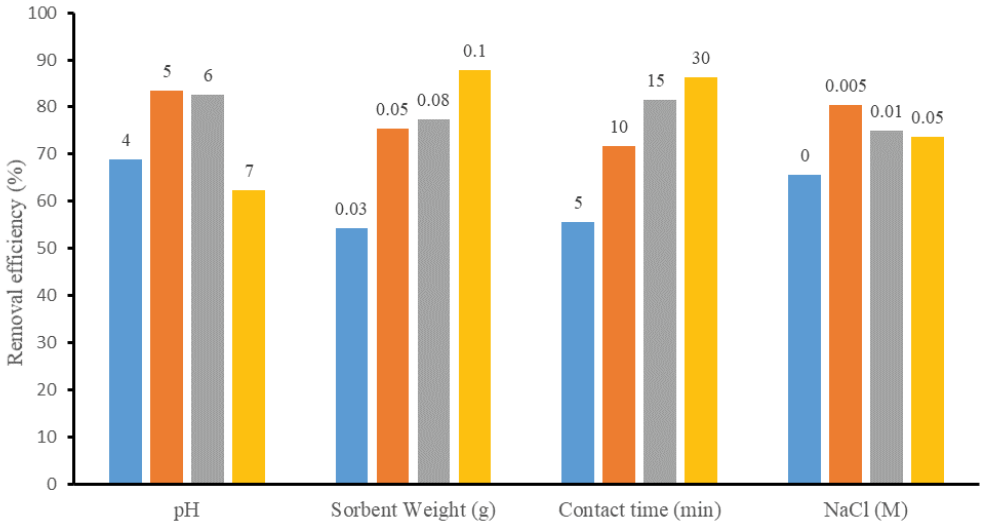

Fig. 4. Effect of some sorption experimental variables on the chlorpyrifos removal (50 mL solution containing 25 mg·L^{-1} chlorpyrifos).

According to the findings, 0.1 g (2.0 g·L^{-1}) of adsorbent was shown to be the best value, with mean removal efficiency of 87.8%. With increasing the adsorbent amounts, more adsorption sites are available to constant quantities of molecules. It has been shown that if the quantity of the adsorbent is smaller than the optimum amount, the molecules quickly cover the surface of the adsorbent, leaving no surface for further pesticide molecules to adsorb. As a result, some pesticide stays in the solution as unadsorbed.

The influence of ionic strength of the solution on chlorpyrifos removal was examined by adding different amounts of NaCl in the concentration range of 0 to 0.05 mol·L^{-1}. According to Fig. 4, with addition of NaCl concentration up to 0.005 mol·L^{-1}, the pesticide removal increases significantly and improves to 80.49%, which is the maximum obtained efficiency. The increase in removal efficiency with enhancing ionic strength up to 0.005 mol·L^{-1} can be related to the salting-out effect of NaCl in decreasing the analyte's solubility in the aqueous phase. At higher concentrations of NaCl, the removal efficiency was decreased due to the change in the Nernst diffusion film around the adsorbate and reduction in the diffusion rates of chlorpyrifos from the bulk solution onto the adsorbent surface. Therefore, 0.005 mol·L^{-1} of NaCl was chosen as the optimum value.

The contact time has a direct relationship with the adsorption capacity and pesticide removal efficacy. The adsorption process always achieves equilibrium over time. As a result, it is vital to optimize the contact time between the adsorbent and the adsorbate. Fig. 4 shows the study of the contact time on chlorpyrifos adsorption. As shown, the maximum chlorpyrifos adsorption efficiencies were obtained after 30 min, whereas the lowest efficiency was observed after 5 min.

3.4. Analysis of variance

The results of analysis of variance for the removal of chlorpyrifos with the Fe_3O_4@PMA MNPs are shown in Table 2. The experimental results showed that the independent factors, such as pH, adsorbent weight, contact time, and ionic strength, affect the adsorption process. As shown in Table 2, the Fisher ratios (*F*-value) of parameters that were calculated via dividing the variance of each parameter by the variance of error are less than the critical *F* (3,3) value at the 95% confidence level (p = 0.05) which is 9.28 ($F < F_{Table}$). This indicates the parameters have no significant effects on the removal efficiency. Also, according to the results, the greatest effect is related to the sorbent mass and then the contact time, the pH, and the ionic strength, respectively.

Table 2
Analysis of variance results of experimental data

Source	df	Sum of squares	Variance	*F*-value
pH	3	1,142.3578	380.78592	2.5241
Sorbent mass	3	2,357.1141	785.70471	5.2081
Contact time	3	2,205.0625	735.02082	4.8721
Ionic strength	3	448.26797	149.42266	0.9905
Error	3	452.5859	150.86196	–
Total	15	6,605.3882	–	–

The critical *F* (3,3) value at the 95% confidence level (p = 0.05) is equal to 9.28.

3.5. Studies on the adsorption kinetics

Kinetic parameters are utilized to anticipate the quantity of adsorption. They also provide valuable information for adsorption process design and modeling [35]. Kinetic studies were carried out by stirring the adsorption mixture at various predetermined time intervals 0.5, 1, 3, 5, 10, 15, 30, and 45 min at the optimum conditions: pH = 5, ionic strength = 0.005 mol·L^{-1}, adsorbent mass = 0.1 g, volume of sample = 50 mL at ambient temperature at two concentration levels of 5 and 25 mg·L^{-1}. A magnet was used to separate the adsorbent from the remaining solution, and the absorbance of the residual solution was measured spectrophotometrically. The residual amounts of chlorpyrifos in the solution were calculated from the proper calibration curve, and the adsorption capacity at time t (q_t, mg·g^{-1}) was obtained from the following equation [Eq. (2)]:

$$q_t = \frac{\left(C_0 - C_t\right)V}{m} \tag{2}$$

where V is the solution volume (L), and m is the mass of the adsorbent (g). C_0 and C_t are the initial and equilibrium concentrations (mg·L^{-1}) of chlorpyrifos at time t, respectively. The adsorption kinetics were investigated using the linear and non-linear forms of pseudo-first-order, pseudo-second-order, Elovich, and intraparticle diffusion models. For the best fitting and finding the parameters of adsorption models, linear regression analysis and the least squares method are frequently used. The kinetic and isotherm models can be easily solved by linearization, where the linear regression coefficient (R^2) is commonly used as indicative of model fitting. In linear forms, the R^2 values closest to unity have been assumed to provide the best fitting. During the transformations of non-linear equations to linear forms, the error structure can be altered. Therefore, the non-linear analysis is used in order to avoid errors raised by different estimates resulting from simple linear regression of the linearized forms which can affect R^2 values significantly. In non-linear forms, Chi-square (χ^2) was used in order to evaluate the fitting of models by measuring the difference between experimental and model-calculated equilibrium adsorption data. If data from the model are similar to the experimental, χ^2 will be a small number. Very small χ^2 test means that calculated data fitted extremely well with experimental data.

The pseudo-first-order kinetic model (Table 3) shows the penetration occurs within a boundary layer and variations in the quantity of adsorption over time is proportional to the number of unoccupied sites on the adsorbent surface. Due to the inappropriate R^2 values, it can be concluded that the pseudo-first-order model is not the proper kinetic model for interpreting the kinetic data. The adsorption capacity-based pseudo-second-order kinetic model (Table 3) shows that sorption process is controlled by diffusion into a network of small pores as the rate-limiting step. Therefore,

diffusion appears to play a crucial role in determining the rate of adsorption onto and into the porous particles [26]. The Elovich model (Table 3) is more suitable for chemical adsorption kinetics and systems with heterogeneous surfaces [36]. Multi-stage adsorption (transfer of adsorbed molecules from the aqueous phase to the surface of solid particles, followed by penetration of solute molecules into the interior of solid particles) and competitive adsorptions are described by intraparticle diffusion (Table 3), which is one of the diffusion-based kinetic models [37].

The quantity of pesticide adsorbed on the adsorbent at equilibrium and at time t, in mg·g^{-1}, are denoted by q_e and q_t, respectively. The value of k_1 (min^{-1}), is determined from the slop of the linear form of the pseudo-first-order model by graphing $\log(q_e - q_t)$ against t (Fig. 5c and d). The pseudo-second-order kinetic constant (k_2, g·mg^{-1}·min^{-1}), and the equilibrium adsorption capacity (q_e, mg·g^{-1}) are determined from the intercept and the slope of the t/q_t vs. t linear graph, respectively (Fig. 5e and f). The initial adsorption rate constant (a, mg·g^{-1}·min^{-1}) in the Elovich model, and the desorption factor (b, g·mg^{-1}), are calculated by drawing the q_t vs. ln$t$ (Fig. 5g and h). K_p and C (mg·g^{-1}) are the intraparticle slope and intercept, respectively, indicating the rising or falling the intraparticle penetration (Fig. 6). The good R^2 values of the pseudo-second-order kinetic model in its linear form ($R^2 > 0.99$) and the results of the other kinetic models (Table 4) reveal that this model can accurately explain the kinetics of the adsorption process. This indicates the diffusion appears to play a crucial role in determining the rate of adsorption onto the porous particles.

3.6. Studies on the adsorption isotherms

Adsorption isotherms reflect the equilibrium connection between the amount of adsorbed material and its equilibrium concentration in solution at a constant temperature. All isotherm studies were investigated using 0.1 g adsorbent and 50 mL chlorpyrifos solution with different

Table 3
Linear and non-linear forms of kinetic models

Kinetic model	Non-linear form	Plot	Linear form	Plot
Pseudo-first-order	$q_t = q_e\left(1 - e^{-k_1 t}\right)$	q_e vs. C_e	$\log\left(q_e - q_t\right) = \log q_e - \frac{k_1 t}{2.303}$	$\log(q_e - q_t)$ vs. t
Pseudo-second-order	$q_t = \frac{k_2 q_e^2 t}{1 + k_2 q_e t}$	q_t vs. t	$\frac{t}{q_t} = \frac{1}{k_2 q_e^2} + \left(\frac{1}{q_e}\right)t$	t/q_t vs. t
Elovich	$q_t = \frac{1}{b}\ln\left(abt + 1\right)$	q_t vs. t	$q_t = \frac{1}{b}\ln\left(ab\right) + \frac{1}{b}\ln t$	q_t vs. ln$t$
Intraparticle diffusion	$q_t = k_p t^{0.5} + C$	q_t vs. t	$q_t = k_p t^{0.5} + C$	q_t vs. $t^{0.5}$

Table 4
Parameters of kinetic models for chlorpyrifos by the Fe_3O_4@PMA MNPs

Kinetic model	Parameters for linear form			Parameters for non-linear form		
	Parameters	5 (mg·L^{-1})	25 (mg·L^{-1})	Parameters	5 (mg·L^{-1})	25 (mg·L^{-1})
Pseudo-first-order	R^2	0.679	0.7783	Adjusted R^2	0.7879	0.9733
	q_e (mg·g^{-1})	0.415	3.588	q_e (mg·g^{-1})	0.9411	10.94
	k_1 (min^{-1})	0.033	0.1025	k_1 (min^{-1})	0.9569	0.553
				Reduced χ^2	0.0152	0.3446
Pseudo-second-order	R^2	0.9910	0.9942	Adjusted R^2	0.7977	0.9125
	q_e (mg·g^{-1})	1.11	11.31	q_e (mg·g^{-1})	1.0206	11.94
	k_2 (g·mg^{-1}·min^{-1})	0.45	0.10	k_2 (g·mg^{-1}·min^{-1})	1.1742	0.0611
				Reduced χ^2	0.0145	1.1268
Elovich	R^2	0.7567	0.7853	Adjusted R^2	0.7122	0.7348
	a (mg·g^{-1}·min^{-1})	0.22	25.70	a (mg·g^{-1}·min^{-1})	6.3619	0.5084
	b (g·mg^{-1})	0.82	0.49	b (g·mg^{-1})	6.8610	26.9224
				Reduced χ^2	0.0206	3.4157
Intraparticle diffusion	R^2	0.5889	0.5149	Adjusted R^2	0.5204	0.4341
	K_p (mg·g^{-1}·min$^{-0.5}$)	0.09	1.20	K_p (mg·g^{-1}·min$^{-0.5}$)	0.0960	1.204
	C (mg·g^{-1})	0.51	4.92	C (mg·g^{-1})	0.5116	4.93
				Reduced χ^2	0.0344	7.2889

concentrations (0.5–100 mg·L^{-1}) at 298 K. These solutions were adjusted at an optimum pH of 5 and 0.005 mol·L^{-1} ionic strength and agitated on a stirrer for adsorption process (30 min). The quantity of chlorpyrifos adsorbed was derived from Eq. (2). The best-fit isotherm model was determined by carrying out both linear and non-linear regressions of Langmuir, Freundlich, Temkin and Dubinin–Radushkevich isotherm equations. The compliance of the adsorption data with four isothermal models was evaluated after magnetic separation of adsorbent. The Langmuir adsorption isotherm (Table 5) assumes that adsorption occurs at specific homogeneous sites in the adsorbent, that each site is occupied by a molecule. This model assumes that adsorption occurs as a single layer on the adsorbent's free surface. Unlike the Langmuir model, Freundlich's adsorption isotherm (Table 5) as an empirical model examines multilayer and reversible adsorption on the heterogeneous surfaces. In this model, the adsorption energy decreases exponentially as the adsorption centers of an adsorbent are occupied. Temkin isotherm is applied to investigate the role of indirect adsorbate/adsorbate interactions in an adsorption process. By ignoring the extremely low and large values of concentrations, it is also assumed that the heat of adsorption of all molecules in the layer decreases linearly as a result of increased surface coverage. The Temkin isotherm (Table 5) has a component that shows how adsorbed and adsorbent particles interact. The Dubinin–Radushkevich isotherm (Table 5) is used to calculate thermodynamic parameters and is based on adsorption on heterogeneous surfaces.

In Table 5, C_e and q_e are the equilibrium liquid phase concentration of adsorbate (mg·L^{-1}) and the amount of adsorbed per gram of the adsorbate at equilibrium (the adsorption capacity, mg·g^{-1}), respectively. q_{max} indicates the maximum monolayer coverage capacity (mg·g^{-1}), K_L represents the Langmuir isotherm equilibrium constant (L·mg^{-1}), which is related to the surface energy of adsorbent, calculated by drawing C_e/q_e vs. C_e (Fig. 7a). The Freundlich isotherm constant K_F (mg$^{(1-1/n)}$·L$^{1/n}$·g^{-1}) is temperature-dependent and measures the quantity of chemical adsorbed on the adsorbent. In this model, adsorption is considered promising if the value of K_F is found in the range of 1–20, and n is the adsorption intensity (heterogeneity factor) indicating the favorability of the adsorption when it lies between 0 and 10. The value of $1/n$ lower than 1 represents a normal Freundlich isotherm, while cooperative adsorption has larger values. The results of this study reveal that K_F (1.303×10^{-7}) and n values (0.056) were out of these ranges confirmed the Freundlich isotherm cannot fit to the obtained data (Fig. 7b). In Temkin isotherm, A and b represent the Temkin isotherm equilibrium binding constant (L·g^{-1}) and the constant associated with the heat of sorption (J·mol^{-1}), respectively (Fig. 7c). In the Dubinin–Radushkevich equation, q_e, K_{DR}, q_s and ε are the adsorbed chemical per the adsorbent mass (mg·g^{-1}), Dubinin–Radushkevich isotherm constant (mol^2·J^{-2}) as a constant related to the mean free energy of adsorption per mol of the adsorbate, the theoretical isotherm saturation capacity (mg·g^{-1}), and Polanyi potential (J·mol^{-1}), respectively (Fig. 7d). The results of calculations and the correlation coefficient (Table 6) indicate more compliance of adsorption data from and Dubinin–Radushkevich isotherm. Using Fig. 7d and Eq. (13), E (J·mol^{-1}) as the mean free energy of adsorption per molecule of the adsorbate when transferred to the surface of the solid was calculated as 158.11 J·mol^{-1}.

3.7. Thermodynamic study of chlorpyrifos adsorption on the Fe_3O_4@PMA MNPs

Temperature influences the adsorption process by varying the solubility of adsorbate as well as the adsorption process of adsorbate to the adsorbent surface. The

Table 5
Linear and non-linear forms of isotherm models

	Non-linear form	Plot	Linear form	Plot
Langmuir model	$q_e = q_{max}\frac{K_L C_e}{1+K_L C_e}$	q_e vs. C_e	$\frac{C_e}{q_e} = \frac{1}{K_L q_{max}} + \frac{C_e}{q_{max}}$	C_e/q_e vs. C_e
Freundlich model	$q_e = K_F C_e^{1/n}$	q_e vs. C_e	$\log q_e = \log K_F + \frac{1}{n}\log C_e$	$\log q_e$ vs. $\log C_e$
Temkin model	$q_e = \frac{RT}{b}\ln(AC_e)$	q_e vs. C_e	$q_e = \frac{RT}{b}\ln A + \frac{RT}{b}\ln C_e$	q_e vs. $\ln C_e$
Dubinin–Radushkevich model	$q_e = q_s e^{-K_{DR}\varepsilon^2}$	q_e vs. ε^2	$\ln q_e = \ln q_e - K_{DR}\varepsilon^2$ $\varepsilon = RT\ln\left(1+\frac{1}{C_e}\right)$ $E = \frac{1}{\sqrt{2K_{DR}}}$	$\ln q_e$ vs. ε^2

C_e = equilibrium concentration of adsorbate (mg·L^{-1}); q_e = amount of adsorbed per gram of the adsorbent at equilibrium (mg·g^{-1}); q_{max} = maximum monolayer coverage capacity (mg·g^{-1}); K_L = Langmuir isotherm equilibrium constant (L·mg^{-1}) which is related to the surface energy of adsorbent; K_F = Freundlich isotherm constant (mg·g^{-1}); A_T = Temkin isotherm equilibrium binding constant (L·g^{-1}); b = constant related to heat of sorption (J·mol^{-1}); R = universal gas constant (8.314 J·mol^{-1}·K^{-1}); T = temperature at 298 K; q_s = theoretical isotherm saturation capacity (mg·g^{-1}); K_{DR} = Dubinin–Radushkevich isotherm constant (mol^2·J^{-2}); ε = Dubinin–Radushkevich isotherm constant.

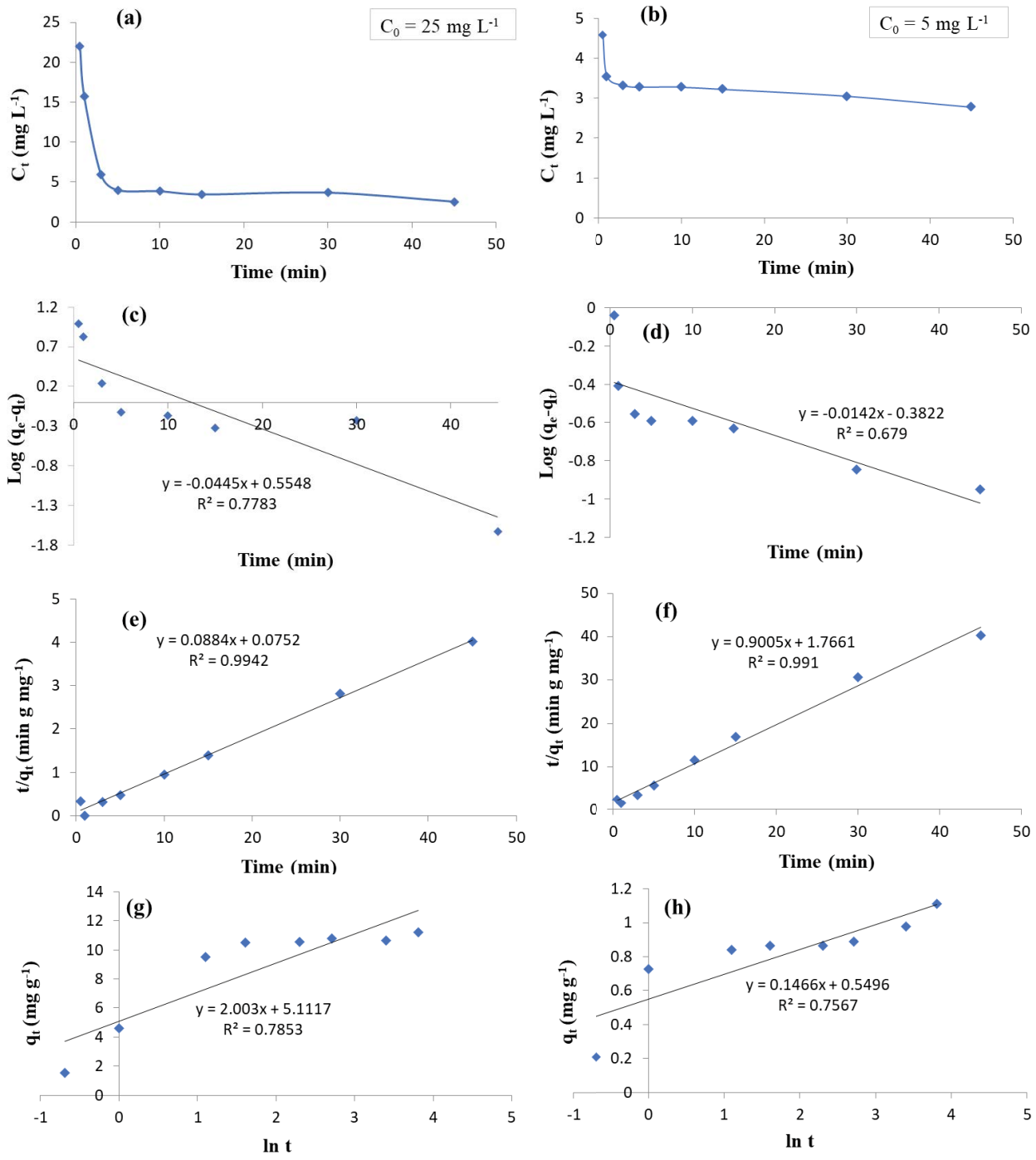

Fig. 5. Chlorpyrifos residual concentration vs. time (a = 25 mg L^{-1} and b = 5 mg L^{-1}), pseudo-first-order (c = 25 mg·L^{-1} and d = 5 mg·L^{-1}), pseudo-second-order (e = 25 mg·L^{-1} and f = 5 mg·L^{-1}), and Elovich (g = 25 mg·L^{-1} and h = 5 mg·L^{-1}) kinetic plots for the chlorpyrifos adsorption onto the synthesized magnetite nanoparticles.

thermodynamic of adsorption reflects the spontaneity or non-spontaneity of processes, the change in entropy of the adsorption process, and whether the adsorption process is endothermic or exothermic. To investigate the temperature effects on the chlorpyrifos adsorption, the experiments were conducted using 25 mg·L^{-1} chlorpyrifos solutions in the temperature range of 25°C–55°C (298.15–328.15 K) at the optimum conditions (sample volume = 50 mL, adsorbent mass = 0.1 g, solution pH = 5, ionic strength = 0.005 mol·L^{-1} and contact time = 30 min). The residual pesticide concentration was determined and the relevant calculations were done after separating the adsorbent and reading the absorbance of the residual solution (Table 7). The following equations are the adsorption thermodynamics linear models:

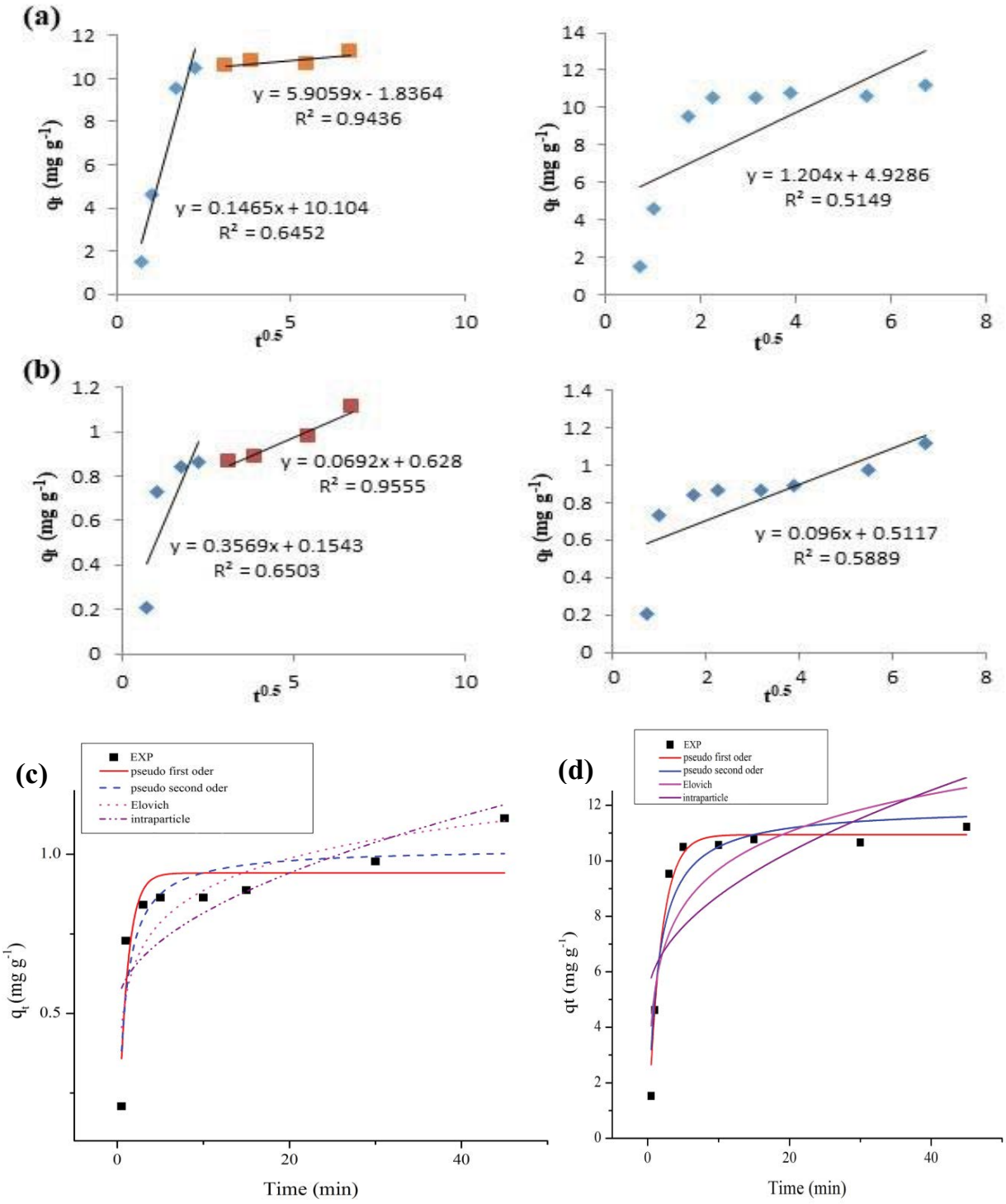

Fig. 6. Intraparticle diffusion linear (a = 25 mg·L^{-1} and b = 5 mg·L^{-1}) and non-linear (c = 5 mg·L^{-1} and d = 25 mg·L^{-1}) kinetic plots for the chlorpyrifos adsorption onto the synthesized magnetite nanoparticles.

$$\ln K = -\frac{\Delta H^\circ}{RT} + \frac{\Delta S^\circ}{R} \quad (3)$$

$$\Delta G^\circ = -RT \ln K \quad (4)$$

$$\Delta G^\circ = \Delta H^\circ - T\Delta S^\circ \quad (5)$$

where R denotes gas constant (J·mol^{-1}·K^{-1}), T represents temperature (K) and K shows the equilibrium constant, that is, expressed as q_e/C_{eq}, indicates the tendency of adsorbate

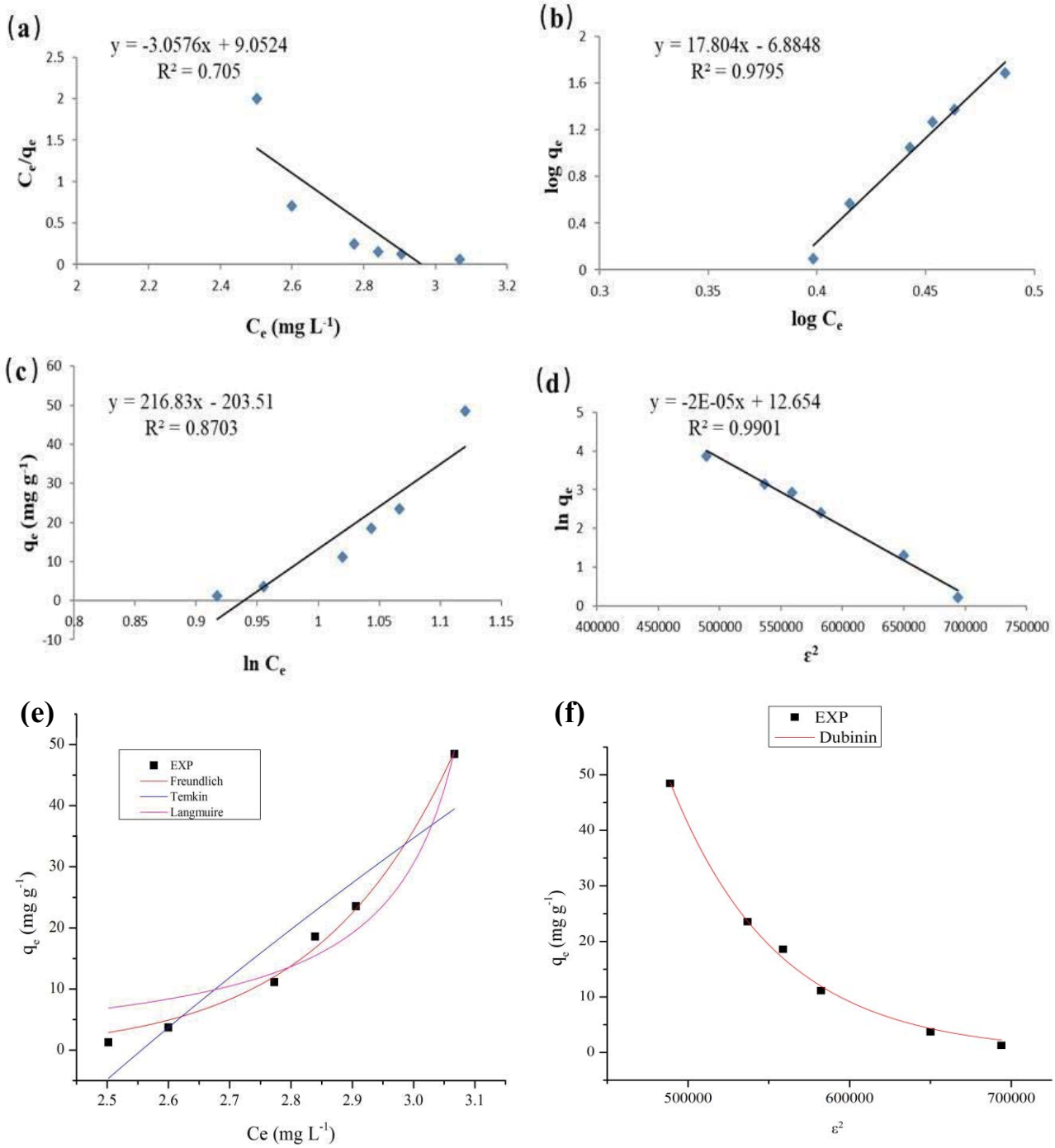

Fig. 7. Linear (a) Langmuir, (b) Freundlich, (c) Temkin, (d) Dubinin–Radushkevich and non-linear isotherm plots (e and f) for the adsorption of chlorpyrifos.

to be hold on the surface of adsorbent and measures the motion of the adsorbate within the solution.

The enthalpy and entropy of the adsorption reaction were calculated using the Van't Hoff equation by plotting ln$K$ in terms of 1/T (Eq. 3). The sign of Gibb's free energy change ($\Delta G°$) shows the spontaneous ($\Delta G° < 0$) or non-spontaneous ($\Delta G° > 0$) nature of the process [26]. The enthalpy change ($\Delta H°$) distinguishes between physical and chemical adsorption and also endothermic ($\Delta H° > 0$) and exothermic processes ($\Delta H° < 0$) [26]. The entropy change ($\Delta S°$) estimates the extent of variations of the adsorbent surface. Table 7 shows the computed values for each of the model's parameters.

From the above equations, $\Delta H°$, $\Delta S°$ and $\Delta G°$ were obtained as 9.665 kJ·mol^{-1}, 40.25 J·mol^{-1}·K^{-1}, and –1.926 kJ·mol^{-1}, respectively. According to the obtained data

Table 6
Parameters of isotherm models (linear and non-linear forms) for chlorpyrifos by the Fe_3O_4@PMA MNPs

Isotherm model	Parameters for linear form		Parameters for non-linear form	
Langmuir	Linear form	$\frac{C_e}{q_e}=\frac{1}{K_L q_{max}}+\frac{C_e}{q_{max}}$	Non-linear form	$q_e=q_{max}\frac{K_L C_e}{1+K_L C_e}$
	R^2	0.70	Adjusted R^2	0.9318
	q_{max} (mg·g^{-1})	0.32	$\lvert q_{max}\rvert$ (mg·g^{-1})	1.874
	K_L (L·mg^{-1})	0.33	K_L (L·mg^{-1})	–0.314
			Reduced χ^2	20.3503
Freundlich	Linear form	$\log q_e=\log K_F+\frac{1}{n}\log C_e$	Non-linear form	$q_e=K_F C_e^{1/n}$
	R^2	0.97	Adjusted R^2	0.9927
	n	0.056	n	0.07177
	K_F (mg$^{(1-1/n)}$·L$^{1/n}$·g^{-1})	1.303 × 10^{-7}	K_F (mg$^{(1-1/n)}$·L$^{1/n}$·g^{-1})	8.0897
			Reduced χ^2	2.1877
Temkin	Linear form	$q_e=\frac{RT}{b}\ln A+\frac{RT}{b}\ln C_e$	Non-linear form	$q_e=\frac{RT}{b}\ln\left(AC_e\right)$
	R^2	0.87	Adjusted R^2	0.8378
	A (L·g^{-1})	0.39	A (L·g^{-1})	0.3912
	b (J·mol^{-1})	11.43	b (J·mol^{-1})	11.43
			Reduced χ^2	48.3793
Dubinin–Radushkevich	Linear form	$\ln q_e=\ln q_s-K_{DR}\varepsilon^2$ $\varepsilon=RT\ln\left(1+\frac{1}{C_e}\right)$ $E=\frac{1}{\sqrt{2K_{DR}}}$	Non-linear form	$q_e=q_s e^{-K_{DR}\varepsilon^2}$
	R^2	0.99	Adjusted R^2	0.9961
	E (J·mol^{-1})	158.11	E (J·mol^{-1})	182.27
	q_s (mg·g^{-1})	12.654	q_s (mg·g^{-1})	76,714.5
	K_{DR} (mol^2·J^{-2})	2E-05	K_{DR} (mol^2·J^{-2})	1.506E-05
			Reduced χ^2	1.1507

(Table 7), with increasing the temperature, the chlorpyrifos adsorption on the Fe_3O_4@PMA MNPs is improved, indicating the removal of chlorpyrifos from the solution is endothermic. The positive $\Delta S°$ shows an increase in the randomness at the interface of the solution-adsorbent with the progress of the sorption process. The negative $\Delta G°$ value indicates the spontaneous nature of chlorpyrifos sorption on the surface of adsorbent. The increase in $\Delta G°$ value by raising the temperature (Table 7) shows that the sorption process is favorable at higher temperatures. The magnitude of $\Delta H°$ and $\Delta G°$ distinguish between physisorption and chemisorption. In this study, the obtained value of $\Delta G°$ from Eq. (5) (–2.326 kJ·mol^{-1} at 298 K) revealed that the sorption process is physisorption and involves a weak force of attraction (typically physisorption yields $\Delta G°$ value with the range of 0 to –20 kJ·mol^{-1} while the $\Delta G°$ for chemisorption lies between –80 to –400 kJ·mol^{-1}) [38]. The obtained $\Delta H°$ value (9.665 kJ·mol^{-1}) confirmed the physisorption process (typically physisorption yields $\Delta H°$ value lower than –80 kJ·mol^{-1} while the $\Delta H°$ for chemisorption lies between –80 to –200 kJ·mol^{-1}) [38–41]. The activation energy (E_a) and sticking probability (S^*) of adsorption were estimated using the modified Arrhenius equation related to the surface coverage (θ) as Eqs. (6)–(9) [42].

Table 7
Thermodynamic parameters for the adsorption of chlorpyrifos

$\Delta G°$ (kJ·mol^{-1})	K	T (K)	$\Delta S°$ (J·mol^{-1}·K^{-1})	$\Delta H°$ (kJ·mol^{-1})
–1.926	2.176	298	40.25	9.665
–2.543	2.700	308		
–2.757	2.838	318		
–3.225	3.263	328		

$$\theta=1-\frac{C_e}{C_0} \tag{6}$$

$$S^*=\left(1-\theta\right)e^{-E_a/RT} \tag{7}$$

$$\ln S^* = \ln(1-\theta) - \frac{E_a}{RT} \quad (8)$$

$$\ln(1-\theta) = \ln S^* + \frac{E_a}{RT} \quad (9)$$

The E_a and S^* were obtained from the slope and intercept of the plot ln(1–θ) vs. 1/T. The positive E_a (8.677 kJ·mol^{-1}) confirmed the endothermic nature of the adsorption process which is in agreement with enthalpy results that showed the endothermic adsorption process. According to the previous studies, the physical or chemical nature of adsorption process can be concluded from the magnitude of E_a. The low E_a values (5–40 kJ·mol^{-1}) shows physical sorption, while the higher E_a values (40–800 kJ·mol^{-1}) confirm chemisorption process [42–44]. In this research, the obtained E_a confirmed the physisorption mechanism. The sticking probability (S^*) as an indication of the probability of sticking of chlorpyrifos to the surface was obtained as 0.0055, which indicates the probability of sticking to the surface is high, when $0 < S^* < 1$ it shows the adsorption process is preferable [42–44].

3.8. Study of chlorpyrifos desorption from Fe_3O_4@PMA MNPs

In order to investigate the desorption of chlorpyrifos adsorbed on the surface of synthesized Fe_3O_4@PMA MNPs, repetitive removal experiments were done at the optimum conditions using the same adsorbent. After the adsorption process using the super magnet, the MNPs were separated from the residual solution and the desorption ability of EtOH, MeOH and distilled water were investigated by adding three different volumes of each eluent (1.5, 2 and 3 mL) to the MNPs and mixing them for a period of time. The results showed the desorption ability of the solvents lies in the order of EtOH > MeOH > distilled water. Therefore, adsorbed chlorpyrifos was eluted from the surface of Fe_3O_4@PMA MNPs, using 2 mL EtOH (for 10 min desorption time).

3.9. Discussion

pH, which impacts the surface charge of the adsorbent and the adsorption process, is one of the most critical chemical parameters in chlorpyrifos adsorption. Based on the findings, the acidic range has the maximum removal efficacy of chlorpyrifos. At pH = 5, the strongest electrostatic interaction between pesticide and adsorbent occurs, resulting in the highest adsorption capacity [45]. The optimal removal efficiency was found at pH = 5 in a study conducted by Affam and Chaudhuri [46] for the breakdown of chlorpyrifos, cypermethrin, and phlorotannin pesticides in aqueous solutions utilizing UV photons and TiO_2 catalyst. The contact duration between the adsorbent and the solution should be extended to improve the quantity of adsorption as well as the likelihood of more pesticide interaction with the functional groups in the adsorbent structure [47]. With increasing time, more adsorbent particles are available to participate in the adsorption process and reaction. The contact time in this study is in agreement with the Rahdar and Ahmadi's findings. In research published in 2020 by Rahdar and Ahmadi, aniline adsorption was boosted by extending the exposure time from 10 to 30 min, resulting in a removal effectiveness of 95.7% after 30 min. This rise in adsorption is because of an increase in the number of collisions between the pollutants and the adsorbent at the longer contact times [48,49]. The removal rate increases as the amount of adsorbent is increased, which is due to the large number of active sites available to the adsorbent, and the active surface of the adsorbent, as well as dynamic factors like increasing free bands on the adsorbent and increasing collision rate [50]. With rising compound concentration and at a fixed quantity of adsorbent, the removal rate of chlorpyrifos falls. The removal effectiveness diminishes as the concentration rises because fewer active sites remain on the adsorbent surface to absorb the pesticide. The active site of the adsorbent is not a limiting factor at lower pesticide concentrations [51]. The removal of chlorpyrifos diminishes as the starting concentration rises, which is likely owing to adsorbent site saturation, resulting in a reduction in the effective amount of adsorbent and consequently a reduction in adsorption efficiency. Maldonado found that when the levels of the poisons including alachlor, atrazine, and chlorpyrifos rise, the removal efficiency drops [52]. Moreover, Chaudhary et al. [53] found that the removal effectiveness reduces as the original pollutant concentration rises. The study of adsorption kinetics identifies the adsorption mechanism as well as its adsorption capacity with time and estimates the adsorption speed. The process follows a pseudo-first-order kinetic model, if the adsorption process is constrained to a reversible process by penetration through the adsorbent boundary layer [54]. The bonds are dependent on the difference in pressure between the contaminant and the adsorbent surface, or the reaction rate at the concentration, according to the pseudo-first-order kinetic model [55]. In the pseudo-second-order kinetic model, the adsorption process is dependent on the solid-phase adsorption. Furthermore, the adsorption capacity is related to the adsorbent's active sites [54]. The pseudo-second-order kinetic model is more consistent and adequate for modeling chlorpyrifos uptake than other models (R^2 = 0.99), according to the correlation coefficients in this study. Wang et al. [55] used methyl orange and Omido Black 10B to eliminate porous chitosan-doped graphene oxide. The results revealed that the adsorption process follows pseudo-second-order kinetics. In a study conducted by Kamboh et al. [56], Calypso Arne-based magnetic sporopollenin was used to remove organophosphate herbicides from water. At pH = 7, with a contact period of 10 min, the chlorpyrifos removal efficiency was 96% and diazinon removal efficiency was 88%. The results revealed that chlorpyrifos and diazinon adsorption follows the Langmuir and Dubinin–Radushkevich isotherms. The physisorption nature of adsorption in the present research is in agreement by Kouchakinejad et al. [26] study on using Fe_3O_4@SiO_2@SBA-3-SO_3H core-shell mesoporous magnetic nanoparticles as an effective adsorbent for paraquat herbicide removal from the aqueous solutions. From the thermodynamic studies, they calculated $\Delta H°$, $\Delta S°$, $\Delta G°$, and E_a of adsorption process as –4,697.08 J·mol^{-1}, –3,938 J·mol^{-1}·K^{-1}, –3,523.45 J·mol^{-1} and –4,246.46 J·mol^{-1}, respectively. The negative $\Delta H°$ and $\Delta G°$ values indicated the exothermic and spontaneous nature of paraquat sorption on the surface of

Table 8
Comparison of kinetics and isothermic models of synthesized Fe_3O_4@PMA MNPs with other adsorbents for chlorpyrifos removal

Adsorbent	Pesticide	Kinetic model	Isotherm model	q_{max} (mg·g^{-1})	References
CuCH[a]	Malathion	Pseudo-second-order	–	322.6	[59]
TPAC[b]	Acetampirid	Pseudo-second-order	Langmuir	35.7	[60]
Fe_3O_4@MGO-NGC	Hexaconazole	Pseudo-second-order	Langmuir	93.46	[61]
Fe_3O_4@MGO-NGC	Chlorpyrifos	Pseudo-second-order	Langmuir	78.74	[61]
Calix-EPPTMS-MS[c]	Chlorpyrifos	Pseudo-second-order	Langmuir	9.81	[56]
Calix-EPPTMS-MS	Diazinon	Pseudo-second-order	Dubinin–Radushkevich	9.07	[56]
BNT[S]d	Paraquat	–	Langmuir	11.75	[62]
Fe_3O_4@SiO_2@GO-P[E]Ae	Chlorpyrifos Malathion Parathion	Pseudo-second-order	Sips	–	[63]
Fe_3O_4@SiO_2@SBA-3-SO_3H[f]	Paraquat	Pseudo-second-order	Langmuir	14.73	[26]
Fe_3O_4@PMA MNP**s**	Chlorpyrifos	Pseudo-second-order	Dubinin–Radushkevich	12.65	This research

[a]Copper chitosan nanocomposite; [b]Porous activated carbon from lignocellulosic agricultural waste; [c]Amino-substituted calixarene-based magnetic sporopollenin; [d]Bentonite modified with mesoporous silica; [e]Graphene oxide-based silica coated magnetic nanoparticles functionalized with 2-phenylethylamine; [f]Magnetite nanoparticles decorated by SBA-3-SO_3H mesoporous silica

nanoparticles, respectively. Moreover, the obtained values of $\Delta H°$, $\Delta G°$ and E_a confirmed the physisorption nature of interaction. The calculated sticking probability (S^*) showed the high probability of sticking to the surface. Kumar and Jiang [57] investigated graphene oxide with chitosan as a novel adsorbent for arsenic adsorption from an aqueous solution. A positive value of $\Delta H°$ shows that the process is endothermic and that the quantity of arsenic removal increases as the ambient temperature rises; a negative value of $\Delta G°$ indicates that the reaction is possible and spontaneous. Positive $\Delta S°$ values also imply that during the adsorption process, the degree of unanticipated adsorption on the solid-liquid surface would grow. Hu et al. [58] used a graphene oxide/polypyrrole composite to investigate the removal of phenol and aniline from aqueous solutions. Their finding showed that the elimination of phenol and aniline is a spontaneous and endothermic process. *Acacia nilotica* seed shell ash supported $Ni_{0.5}Zn_{0.5}Fe_2O_4$ MNPs was investigated for adsorption of Pb(II) by Omidvar-Hosseini and Moeinpour [18]. The experimental data were fitted well with the pseudo-second-order kinetic model (R^2 = 0.999) and Langmuir isotherm model (R^2 = 0.900).

The efficiency of Fe_3O_4@PMA MNPs for removal of chlorpyrifos was compared with the q_{max}, kinetic and isotherm models of some of the previous studies that were utilized for the removal of pesticides using nanoparticles (Table 8). This table shows that the Fe_3O_4@PMA MNPs have good adsorption capacity and are comparable with other adsorbents.

4. Conclusion

The efficiency of poly(methacrylic acid) surface-modified iron oxide in removing chlorpyrifos was evaluated in this study. After characterization of the synthesized modified MNPs, the influence of several experimental factors on the adsorption process was investigated, followed by kinetic, isotherm, and thermodynamic studies. The removal of chlorpyrifos by Fe_3O_4@PMA MNPs followed the Dubinin–Radushkevich isotherm and the pseudo-second-order kinetic models. According to the study on the adsorption thermodynamics, chlorpyrifos adsorption on the adsorbent is endothermic and spontaneous. Generally, the findings of this investigation revealed that Fe_3O_4@PMA MNPs had a good adsorption efficiency for removing chlorpyrifos from aqueous solutions.

Acknowledgments

The authors are humbly thankful to Rasht Branch, Islamic Azad University for supporting this study.

Declarations

Ethical approval

This declaration is not applicable.

Competing interests

The authors declare that they have no known competing financial interests or personal relationships that could have appeared to influence the work reported in this paper.

Authors' contributions

Both authors contributed to the design of the review paper, and to the writing of the manuscript.

Funding

There is no founding for supporting this paper.

Availability of data and materials

The data that support the findings of this paper are available from the corresponding author upon reasonable request.

References

[1] T. Ahmad, M. Rafatullah, A. Ghazali, O. Sulaiman, R. Hashim, A. Ahmad, Removal of pesticides from water and wastewater by different adsorbents: a review, J. Environ. Sci. Health., Part C Environ. Carcinog. Ecotoxicol. Rev., 28 (2010) 231–271.

[2] P. Kadam, R. Patil, Effect of chlorpyrifos on some biochemical constituents in liver and kidney of fresh water fish, *Channa gachua* (F. Hamilton), Int. J. Sci. Res., 5 (2016) 1975–1979.

[3] E. Testai, F.M. Buratti, E. Di Consiglio, Chapter 70 – Chlorpyrifos, R. Krieger, Ed., Hayes' Handbook of Pesticide Toxicology (Third Edition), Academic Press, New York, 2010, pp. 1505–1526.

[4] A.A. Chougule, R.S. Brar, H.S. Banga, N.D. Singh, A. Goyal, P.D. Gadhave, Concomitant effect of chlorpyrifos and intranasal endotoxin administration on apoptosis related protein expression in lung of mice, J. Environ. Anal. Toxicol., 3 (2013) 1–5.

[5] Y. Tian, H. Ishikawa, T. Yamaguchi, T. Yamauchi, K. Yokoyama, Teratogenicity and developmental toxicity of chlorpyrifos: maternal exposure during organogenesis in mice, Reprod. Toxicol., 20 (2005) 267–270.

[6] R.S. Verma, A. Mehta, N. Srivastava, *In vivo* chlorpyrifos induced oxidative stress: attenuation by antioxidant vitamins, Pest. Biochem. Phys., 88 (2007) 191–196.

[7] R. Trager, US Bans Chlorpyrifos on all Food Crops, Chemistry World, 2022.

[8] I. Ali, V.K. Gupta, Advances in water treatment by adsorption technology, Nat. Protoc., 1 (2006) 2661–2667.

[9] A. Mojiri, J.L. Zhou, B. Robinson, A. Ohashi, N. Ozaki, T. Kindaichi, H. Farraji, M. Vakili, Pesticides in aquatic environments and their removal by adsorption methods, Chemosphere, 253 (2020) 126–646.

[10] S.S. Banerjee, D.-H. Chen, Fast removal of copper ions by gum arabic modified magnetic nano-adsorbent, J. Hazard. Mater., 147 (2007) 792–799.

[11] S. Shariati, A. Chinevari, M. Ghorbani, Simultaneous removal of four dye pollutants in mixture using amine functionalized kit-6 silica mesoporous magnetic nanocomposite, Silicon, 12 (2020) 1865–1878.

[12] S. Rahnama, S. Shariati, F. Divsar, Synthesis of functionalized magnetite titanium dioxide nanocomposite for removal of acid fuchsine dye, Comb. Chem. High Throughput Screening, 21 (2018) 583–593.

[13] N. Besharati, N. Alizadeh, S. Shariati, Removal of tetracycline from aqueous solution by *Azolla*, fig leaves, eggshell and egg membrane modified with magnetite nanoparticles, Desal. Water Treat., 225 (2021) 214–224.

[14] S. Mousazadeh, S. Shariati, M. Yousefi, S. Baniyaghoob, H. Kefayati, Hexavalent chromium removal using ionic liquid coated magnetic nano zero-valent iron biosynthesized by *Camellia sinensis* extract, Int. J. Environ. Res., 15 (2021) 1017–1036.

[15] F. Tajali Rad, H. Kefayati, S. Shariati, Synthesis of propyl aminopyridine modified magnetite nanoparticles for cadmium(II) adsorption in aqueous solutions, Appl. Organomet. Chem., 33 (2019) e4732, doi: 10.1002/aoc.4732.

[16] S. Shariati, N. Parto, E. Bozorgzadeh, P. Zanjanchi, S. Rahnama, Magnetic solid phase preconcentration of cadmium in water samples using sulfonic acid functionalized kit-6 magnetite mesoporous nanocomposites followed by flame atomic absorption spectrometry, J. Iran. Chem. Soc., 17 (2020) 3375–3382.

[17] P. Beigzadeh, F. Moeinpour, Fast and efficient removal of silver(I) from aqueous solutions using aloe vera shell ash supported $Ni_{0.5}Zn_{0.5}Fe_2O_4$ magnetic nanoparticles, Trans. Nonferrous Met. Soc. China, 26 (2016) 2238−2246.

[18] F. Omidvar-Hosseini, F. Moeinpour, Removal of Pb(II) from aqueous solutions using *Acacia nilotica* seed shell ash supported $Ni_{0.5}Zn_{0.5}Fe_2O_4$ magnetic nanoparticles, J. Water Reuse Desal., 6 (2016) 562–573.

[19] G. Gnanaprakash, S. Mahadevan, T. Jayakumar, P. Kalyanasundaram, J. Philip, B. Raj, Effect of initial pH and temperature of iron salt solutions on formation of magnetite nanoparticles, Mater. Chem. Phys., 103 (2007) 168–175.

[20] A.-H. Lu, E.L. Salabas, F. Schüth, Magnetic nanoparticles: synthesis, protection, functionalization, and application, Angew. Chem. Int. Ed., 46 (2007) 1222–1244.

[21] S. Shariati, M. Khabazipour, F. Safa, Synthesis and application of amine functionalized silica mesoporous magnetite nanoparticles for removal of chromium(VI) from aqueous solutions, J. Porous Mater., 24 (2017) 129–139.

[22] C.C. Berry, A.S.G. Curtis, Functionalisation of magnetic nanoparticles for applications in biomedicine, J. Phys. D: Appl. Phys., 36 (2003) R198–R206.

[23] S. Rahnama, S. Shariati, F. Divsar, Selective aptamer conjugation to silver-coated magnetite nanoparticles for magnetic solid-phase extraction of trace amounts of Pb^{2+} ions, RSC Adv., 11 (2021) 4971–4982.

[24] S. Moradi Dehaghi, B. Rahmanifar, A.M. Moradi, P.A. Azar, Removal of permethrin pesticide from water by chitosan–zinc oxide nanoparticles composite as an adsorbent, J. Saudi Chem. Soc., 18 (2014) 348–355.

[25] B. Karimi, Comparison between nanotechnology and other mehods for removal cypermethrin pesticide in contaminated water, J. Water Wastewater Sci. Eng., 2 (2017) 3–13.

[26] R. Kouchakinejad, S. Shariati, J. Abolhasani, E.G. Kalhor, M.T. Vardini, Core-shells of magnetite nanoparticles decorated by SBA-3-SO_3H mesoporous silica for magnetic solid phase adsorption of paraquat herbicide from aqueous solutions, Colloids Surf., A, 643 (2022) 128709, doi: 10.1016/j.colsurfa.2022.128709.

[27] M. Amiri, R. Rezaee Kalantari, M. Kermani, M. Yeganeh, M. Gholami, Investigation of chlorpyriphos removal using chitosan graphene oxide composite form aquatic solution: study of kinetics, isotherms and thermodynamics, Sci. J. Kurdistan Univ. Med. Sci., 24 (2019) 119–138.

[28] M.H. Dehghani, S. Kamalian, M. Shayeghi, M. Yousefi, Z. Heidarinejad, S. Agarwal, V.K. Gupta, High-performance removal of diazinon pesticide from water using multi-walled carbon nanotubes, Microchem. J., 145 (2019) 486–491.

[29] A. Nejaei, B. Rahmanifar, A. Esmaeilzadeh, Z. Nasouri Gazani, Collagen-based CuO nano particles; a new adsorbent for removal of cypermethrin from water, Fresenius Environ. Bull., 26 (2017) 2739–2746.

[30] Z. Bensaadi, M. Sahmoune, N. Yeddou Mezenner, Adsorptive removal of diazinon: kinetic and equilibrium study, Desal. Water Treat., 57 (2014) 1–10.

[31] S.M.S. Danesh, H. Faghihian, S. Shariati, Sulfonic acid functionalized SBA-3 silica mesoporous magnetite nanocomposite for safranin O dye removal, Silicon, 11 (2019) 1817–1827.

[32] Z. Zeng, J. Yu, Z.-X. Guo, Preparation of carboxyl-functionalized polystyrene/silica composite nanoparticles, Macromol. Chem. Phys., 205 (2004) 2197–2204.

[33] S.T. Ong, C.K. Lee, Z. Zainal, Removal of basic and reactive dyes using ethylenediamine modified rice hull, Bioresour. Technol., 98 (2007) 2792–2799.

[34] H. Qiao, Y. Zhou, F. Yu, E. Wang, Y. Min, Q. Huang, L. Pang, T. Ma, Effective removal of cationic dyes using carboxylate-functionalized cellulose nanocrystals, Chemosphere, 141 (2015) 297–303.

[35] S. Shariati, M. Faraji, Y. Yamini, A.A. Rajabi, Fe_3O_4 magnetic nanoparticles modified with sodium dodecyl sulfate for removal of safranin O dye from aqueous solutions, Desalination, 270 (2011) 160–165.

[36] A. Khaled, A.E. Nemr, A. El-Sikaily, O. Abdelwahab, Removal of Direct N Blue-106 from artificial textile dye effluent using activated carbon from orange peel: adsorption isotherm and kinetic studies, J. Hazard. Mater., 165 (2009) 100–110.

[37] P. Ramachandran, R. Vairamuthu, S. Ponnusamy, Adsorption isotherms, kinetics, thermodynamics and desorption studies of reactive orange16 on activated carbon derived from *Ananas comosus* (L.) carbon, J. Eng. Appl. Sci., 6 (2011) 15–26.

[38] K.S. Obayomi, M. Auta, A.S. Kovo, Isotherm, kinetic and thermodynamic studies for adsorption of lead(II) onto modified Aloji clay, Desal. Water Treat., 181 (2020) 376–384.

[39] Q. Li, Q.Y. Yue, Y. Su, B.Y. Gao, H.J. Sun, Equilibrium, thermodynamics and process design to minimize adsorbent

amount for the adsorption of acid dyes onto cationic polymer-loaded bentonite, Chem. Eng. J., 158 (2010) 489–497.
[40] Y. Chen, Y.Q. Zhang, T.H. Zhang, C.H. Gan, C.Y. Zheng, G. Yu, Carbon nanotube reinforced hydroxyapatite composite coatings produced through laser surface alloying, Carbon, 44 (2006) 37–45.
[41] F.N. Oskui, H. Aghdasinia, M.G. Sorkhabi, Adsorption of Cr(III) using an Iranian natural nanoclay: applicable to tannery wastewater: equilibrium, kinetic, and thermodynamic, Environ. Earth Sci., 78 (2019) 106, doi: 10.1007/s12665-019-8104-8.
[42] T.S. Najim, S.A. Yassin, Removal of chromium from aqueous solution using modified pomegranate peel: mechanistic and thermodynamic studies, E-J. Chem., 6 (2009) S153–S158.
[43] S.E. Abechi, Studies on the mechanism of adsorption of methylene blue onto activated carbon using thermodynamic tools, Sci. World J., 13 (2018) 17–19.
[44] S. Raghav, D. Kumar, Adsorption equilibrium, kinetics, and thermodynamic studies of fluoride adsorbed by tetrametallic oxide adsorbent, J. Chem. Eng. Data, 63 (2018) 1682–1697.
[45] W. Cheng, M. Wang, Z. Yang, Y. Sun, C. Ding, The efficient enrichment of U(VI) by graphene oxide-supported chitosan, RSC Adv., 4 (2014) 61919–61926.
[46] A.C. Affam, M. Chaudhuri, Degradation of pesticides chlorpyrifos, cypermethrin and chlorothalonil in aqueous solution by TiO_2 photocatalysis, J. Environ. Manage., 130 (2013) 160–165.
[47] S. Yavari, N.M. Mahmodi, P. Teymouri, B. Shahmoradi, A. Maleki, Cobalt ferrite nanoparticles: preparation, characterization and anionic dye removal capability, J. Taiwan Inst. Chem. Eng., 59 (2016) 320–329.
[48] V.C. Srivastava, M.M. Swamy, I.D. Mall, B. Prasad, I.M. Mishra, Adsorptive removal of phenol by bagasse fly ash and activated carbon: equilibrium, kinetics and thermodynamics, Colloids Surf., A, 272 (2006) 89–104.
[49] R. Qadeer, A.H. Rehan, A study of the adsorption of phenol by activated carbon from aqueous solutions, Turk. J. Chem., 26 (2002) 357–361.
[50] L. Fan, C. Luo, M. Sun, X. Li, F. Lu, H. Qiu, Preparation of novel magnetic chitosan/graphene oxide composite as effective adsorbents toward methylene blue, Bioresour. Technol., 114 (2012) 703–706.
[51] S. Dehestaniathar, S. Amini, A. Maleki, B. Shahmoradi, N. Reshadmanesh, P. Teymouri, Adsorption of fluoride using diatomite-supported ferric oxide nanoparticles: determination of optimum condition, kinetics, and adsorption isotherms, Iran. J. Health Environ., 9 (2016) 185–196.
[52] M.I. Maldonado, S. Malato, L.A. Pérez-Estrada, W. Gernjak, I. Oller, X. Doménech, J. Peral, Partial degradation of five pesticides and an industrial pollutant by ozonation in a pilot-plant scale reactor, J. Hazard. Mater., 138 (2006) 363–369.
[53] A. Chaudhary, N. Goswami, S. Grimes, Electrolytic removal of hexavalent chromium from aqueous solutions, J. Chem. Technol. Biotechnol., 78 (2003) 877–883.
[54] S. Tabasideh, A. Maleki, B. Shahmoradi, E. Ghahremani, G. McKay, Sonophotocatalytic degradation of diazinon in aqueous solution using iron-doped TiO_2 nanoparticles, Sep. Purif. Technol., 189 (2017) 186–192.
[55] Y. Wang, G. Xia, C. Wu, J. Sun, R. Song, W. Huang, Porous chitosan doped with graphene oxide as highly effective adsorbent for methyl orange and amido black 10B, Carbohydr. Polym., 115 (2015) 686–693.
[56] M.A. Kamboh, W.A.W. Ibrahim, H.R. Nodeh, M.M. Sanagi, S.T.H. Sherazi, The removal of organophosphorus pesticides from water using a new amino-substituted calixarene-based magnetic sporopollenin, New J. Chem., 40 (2016) 3130–3138.
[57] A.S.K. Kumar, S.-J. Jiang, Chitosan-functionalized graphene oxide: a novel adsorbent an efficient adsorption of arsenic from aqueous solution, J. Environ. Chem. Eng., 4 (2016) 1698–1713.
[58] R. Hu, S. Dai, D. Shao, A. Alsaedi, B. Ahmad, X. Wang, Efficient removal of phenol and aniline from aqueous solutions using graphene oxide/polypyrrole composites, J. Mol. Liq., 203 (2015) 80–89.
[59] M. Jaiswal, D. Chauhan, N. Sankararamakrishnan, Copper chitosan nanocomposite: synthesis, characterization, and application in removal of organophosphorous pesticide from agricultural runoff, Environ. Sci. Pollut. Res., 19 (2012) 2055–2062.
[60] S.G. Mohammad, S.M. Ahmed, A.E.-G.E. Amr, A.H. Kamel, Porous activated carbon from lignocellulosic agricultural waste for the removal of acetampirid pesticide from aqueous solutions, Molecules, 25 (2020) 23–39.
[61] H.R. Nodeh, M.A. Kamboh, W.A.W. Ibrahim, B.H. Jume, H. Sereshti, M.M. Sanagi, Equilibrium, kinetic and thermodynamic study of pesticides removal from water using novel glucamine-calix [4] arene functionalized magnetic graphene oxide, Environ. Sci. Processes Impacts, 21 (2019) 714–726.
[62] A. Rasaie, M. Sabzehmeidani, M. Ghaedi, M. Jahromi, A. Sedaratian-Jahromi, Removal of herbicide paraquat from aqueous solutions by bentonite modified with mesoporous silica, Mater. Chem. Phys., 262 (2021) 124–296.
[63] V. Wanjeri, C. Sheppard, A. Prinsloo, J. Ngila, P. Ndungu, Isotherm and kinetic investigations on the adsorption of organophosphorus pesticides on graphene oxide-based silica coated magnetic nanoparticles functionalized with 2-phenylethylamine, J. Environ. Chem. Eng., 6 (2018) 1333–1346.